Modeling, Simulation and Control of Wind Energy Conversion System based on Doubly Fed Induction Generator and Cycloconverter

Abderraouf BOUMASSATA, Djallel KERDOUN
Constantine 1 University, Constantine, 25000 Algeria
a_boumassata@umc.edu.dz

***Abstract*—In this paper, we propose a wind energy conversion system (WECS) at variable speed using a doubly fed induction generator (DFIG) controlled on the rotor side through a cycloconverter. The dynamic behavior of the WECS, including the models of the wind turbine, the DFIG, the cycloconverter, and the power control of this system, is investigated. The power control of this system is applied to achieve the independent control of the active and reactive powers exchanged between the wind generator and the grid. In addition, a maximum power point tracking (MPPT) control is included in the control system to capture the maximum power from the wind. Moreover, the cycloconverter with DFIG are used to test the possibility to operate in two quadrant modes (sub-synchronous and super-synchronous modes). The description of the proposed system is presented with the detailed dynamic modeling equations. The simulation results are presented, to demonstrate the performance and the efficiency of this system.**

***Index Terms*—Cycloconverter, Doubly fed induction generator (DFIG), Maximum power point tracking (MPPT), Wind energy conversion system (WECS).**

I. INTRODUCTION

The use of renewable sources for electric power generation has experienced a huge face lift since the past decade [1]. The main advantage of renewable sources is the absence of harmful emissions. One way of generating electricity from renewable sources is to use wind energy, mainly because it is considered to be clean and economically viable [2].

Wind turbine generators (WTGs) used in wind energy conversion system can be classified into two types: fixed speed wind turbine (FSWT) and variable speed wind turbine (VSWT). For the first one, the generator is connected directly to the grid without any intermediate of Power electronic converters (PECs), and for the last one, the generator is connected through PECs [3-5]. Moreover, WTGs based on VSWT have distinct advantages than the traditional FSWT, such as more effective power capture, lower mechanical stress and less power fluctuation [6].

The DFIG is widely used for VSWT, and it is one of the most important generators for WECS. The main advantage of the DFIG is that the power electronics equipment only carries a fraction of the total power (20–30%) [7-8].

Cycloconverter is a direct AC-AC converter without any intermediate DC link capacitor and it converts a constant voltage of magnitude and frequency to a variable voltage of magnitude and frequency. The basic principle of the cycloconverter was conceived and patented by Hazeltine in 1926 [9]. Cycloconverter is suitable for large AC machines because it has high efficiency owing to the simple construction of the main circuit, which consists only of switching devices [10].

Many papers have been presented with DFIG for WECS. These papers are generally based on conventional back-to-back converter (AC-DC-AC converter) [11-13] and based on a direct AC-AC matrix converter [8], [14-16].

The main inconvenient of the conventional AC-DC-AC converter is the DC link capacitor. Cycloconverter and matrix converter resolved this problem because both of them don't need any DC link capacitor. However, the matrix converter uses bidirectional switches and that make the system more expensive. Whereas, cycloconverter uses thyristors and that make the system cheaper. Moreover, cycloconverter is typically used in low speed (low frequency) applications like rolling mills [17-18], and that's what we need in the rotor side of the DFIG.

In this work, the cycloconverter with DFIG are used to capture the maximum power from the wind, to control independently the active and reactive powers, to test the possibility to operate in two quadrant modes and to reduce the cost of the proposed system.

This paper is organized as follows. First, the description of the studied WECS is presented in Section II. Second, the modeling of the wind turbine and the control of the MPPT are provided in Section III. Third, the DFIG is modeled in Section IV. Next, the modeling of the cycloconverter is given in Section V. Finally, the power control and simulation results are presented in Section VI and VII respectively.

II. DESCRIPTION OF THE STUDIED WECS

The WECS adopted here is shown in Fig. 1. The proposed system is constituted of wind turbine, DFIG, cycloconverter and power control. The stator of the DFIG is connected directly to the grid while the rotor is connected and controlled by three phase cycloconverter. The performance of the proposed system will be tested to prove the MPPT control, the independent control of grid active and reactive powers using stator flux oriented control technique and to test the ability to operate in two quadrant modes (sub-synchronous and super-synchronous modes).

In both modes, the stator active power is generated from the DFIG and delivered to the grid.

Digital Object Identifier 10.4316/AECE.2014.02007

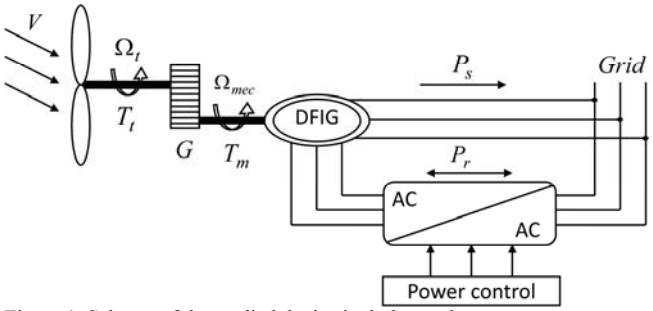

Figure 1. Scheme of the studied device includes cycloconverter

III. MODELING OF THE WIND TURBINE

The mechanical power captured by the turbine from the wind is given by the following expression [19-21]:

$$P_t = \frac{1}{2} \cdot \rho . A . C_p(\lambda, \beta) \cdot V^3 \tag{1}$$

Where ρ is the air density, $A=\pi.R^2$ is the rotor swept area, R is the turbine radius, C_p is the power coefficient, λ is the tip speed ratio, β is the pitch angle and V is the wind speed.

The power coefficient C_p represents the aerodynamic efficiency of the wind turbine. It depends on the tip speed ratio λ and the pitch angle β. The tip speed ratio is given as:

$$\lambda = \frac{\Omega_t \cdot R}{V} \tag{2}$$

With Ω_t is the turbine speed. For our example the power coefficient C_p is given by the following equations [22]:

$$C_p(\lambda, \beta) = a_1 \cdot \sin(a_2) - a_3 \tag{3}$$

$$\begin{cases} a_1 = (0.35 - 0.00167 \cdot (\beta - 2)) \\ a_2 = \dfrac{\pi \cdot (\lambda + 0.1)}{14.34 - 0.3 \cdot (\beta - 2)} \\ a_3 = 0.00184 \cdot (\lambda - 3) \cdot (\beta - 2) \end{cases} \tag{4}$$

Figures 2 and 3 illustrate the curve of C_p (λ, β) obtained by (3) and power-speed characteristics, respectively.

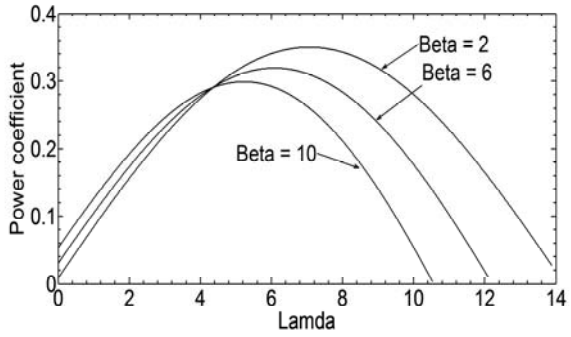

Figure 2. Power coefficient of the wind turbine

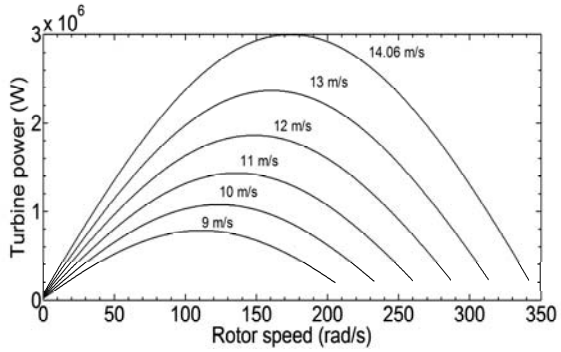

Figure 3. Power-speed characteristics for different wind speeds

The maximum value of C_p (C_{p_max} = 0.35) is for β = 2 degree and for λ = 7.1

The turbine torque can be written as:

$$T_t = \frac{P_t}{\Omega_t} \tag{5}$$

The mechanical speed of the generator and the torque of the turbine referred to the generator are given by:

$$\begin{cases} \Omega_{mec} = \Omega_t \cdot G \\ T_m = \dfrac{T_t}{G} \end{cases} \tag{6}$$

Where G is the gearbox. The mechanical equation of the system can be characterized by:

$$J \frac{d\Omega_{mec}}{dt} = T_m - T_{em} - f \cdot \Omega_{mec} \tag{7}$$

Where J is the equivalent total inertia of the generator shaft, f is the equivalent total friction coefficient and T_{em} is the electromagnetic torque.

In order to capture the optimal mechanical power, the control of the mechanical speed is applied.

Figure 4 represents the diagram blocks of control speed.

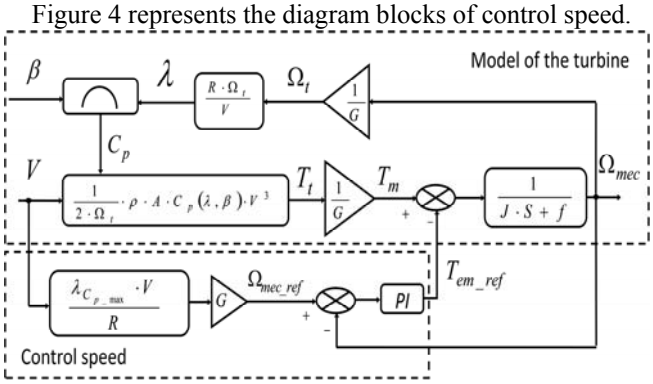

Figure 4. MPPT with the control of the speed

IV. MODELING OF THE DFIG

The electrical equations of the DFIG in the (d–q) Park reference frame are given by [23-24]:

$$\begin{cases} V_{sd} = R_s \cdot I_{sd} + \dfrac{d\phi_{sd}}{dt} - w_s \cdot \phi_{sq} \\ V_{sq} = R_s \cdot I_{sq} + \dfrac{d\phi_{sq}}{dt} + w_s \cdot \phi_{sd} \\ V_{rd} = R_r \cdot I_{rd} + \dfrac{d\phi_{rd}}{dt} - w_r \cdot \phi_{rq} \\ V_{rq} = R_r \cdot I_{rq} + \dfrac{d\phi_{rq}}{dt} + w_r \cdot \phi_{rd} \end{cases} \tag{8}$$

$$\begin{cases} \phi_{sd} = L_s \cdot I_{sd} + M \cdot I_{rd} \\ \phi_{sq} = L_s \cdot I_{sq} + M \cdot I_{rq} \\ \phi_{rd} = L_r \cdot I_{rd} + M \cdot I_{sd} \\ \phi_{rq} = L_r \cdot I_{rq} + M \cdot I_{sq} \end{cases} \tag{9}$$

Where R_s and R_r are, respectively, the stator and rotor resistances. w_s and w_r are the stator and the rotor pulsations, respectively. L_s, L_r and M are, respectively, the cyclic stator, the cyclic rotor and mutual inductances.

The active and reactive powers equations at the stator, the rotor and the grid are, respectively, written as:

$$\begin{cases} P_s = V_{sd} \cdot I_{sd} + V_{sq} \cdot I_{sq} \\ Q_s = V_{sq} \cdot I_{sd} - V_{sd} \cdot I_{sq} \end{cases} \quad (10)$$

$$\begin{cases} P_r = V_{rd} \cdot I_{rd} + V_{rq} \cdot I_{rq} \\ Q_r = V_{rq} \cdot I_{rd} - V_{rd} \cdot I_{rq} \end{cases} \quad (11)$$

$$\begin{cases} P_g = P_s + P_r \\ Q_g = Q_s + Q_r \end{cases} \quad (12)$$

And the electromagnetic torque is expressed as:

$$T_{em} = p \cdot \left(\phi_{sd} \cdot I_{sq} - \phi_{sq} \cdot I_{sd} \right) \quad (13)$$

Where p is the number of pole pairs.

V. Modeling of the Cycloconverter

The cycloconverter is composed of 18 thyristors. Each phase is composed of two rectifiers. The delay angles of those rectifiers are modulated so as to provide an AC output voltage at the desired frequency and amplitude.

Figure 5 represents the model of the cycloconverter.

Each phase has positive converter and negative converter. The first one conducts positive current and the last one conducts negative current. This cycloconverter has natural commutation without circulating current and all thyristors are supposed as idealized.

The switching function in Fig. 5 is defined as:

$$S_{K_{ij}} = \begin{cases} 1 & S_{K_{ij}} \quad is\ closed \\ 0 & S_{K_{ij}} \quad is\ open \end{cases} \quad (14)$$

Where

$$\begin{cases} K \in \{P, N\} \\ i \in \{a, b, c\} \\ j \in \{A, B, C\} \end{cases} \quad (15)$$

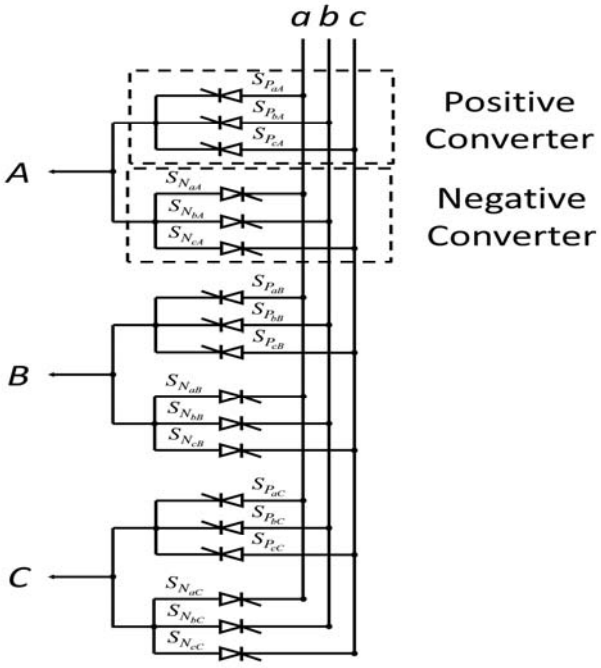

Figure 5. Model of the cycloconverter

At any time (t), only one switch S_{Kij} will be closed in each phase. This assures that no short circuit will be occurring at the input terminals. So, we can express that by the following equation:

$$\begin{cases} S_{P_{aA}} + S_{P_{bA}} + S_{P_{cA}} + S_{N_{aA}} + S_{N_{bA}} + S_{N_{cA}} = 1 \\ S_{P_{aB}} + S_{P_{bB}} + S_{P_{cB}} + S_{N_{aB}} + S_{N_{bB}} + S_{N_{cB}} = 1 \\ S_{P_{aC}} + S_{P_{bC}} + S_{P_{cC}} + S_{N_{aC}} + S_{N_{bC}} + S_{N_{cC}} = 1 \end{cases} \quad (16)$$

In order to control the output voltage of the cycloconverter, we need to command the thyristor firing pulses. In this paper, cosine-wave crossing technique is selected to generate firing pulses (Fig. 6). So we will have three timing waves and three reference waves and a lot of intersection points. We have 18 control circuits for this cycloconverter one for each thyristor. The three phase - three phase cycloconverter can be represented by a 3x3 matrix because switches are connected directly without any intermediate DC link capacitor. Therefore, the output voltage of the cycloconverter can be represented by the transfer function [T] such as:

$$\begin{bmatrix} v_A \\ v_B \\ v_C \end{bmatrix} = [T] \cdot \begin{bmatrix} v_a \\ v_b \\ v_c \end{bmatrix} \quad (17)$$

$$[T] = \begin{bmatrix} \left(S_{P_{aA}} + S_{N_{aA}}\right) & \left(S_{P_{bA}} + S_{N_{bA}}\right) & \left(S_{P_{cA}} + S_{N_{cA}}\right) \\ \left(S_{P_{aB}} + S_{N_{aB}}\right) & \left(S_{P_{bB}} + S_{N_{bB}}\right) & \left(S_{P_{cB}} + S_{N_{cB}}\right) \\ \left(S_{P_{aC}} + S_{N_{aC}}\right) & \left(S_{P_{bC}} + S_{N_{bC}}\right) & \left(S_{P_{cC}} + S_{N_{cC}}\right) \end{bmatrix} \quad (18)$$

Where v_a , v_b and v_c are, respectively, the input phase voltages. v_A, v_B and v_C are, respectively, the output phase voltages.

Figure 6 illustrates the output waveform of the cycloconverter in case of output frequency = (1/10) input frequency.

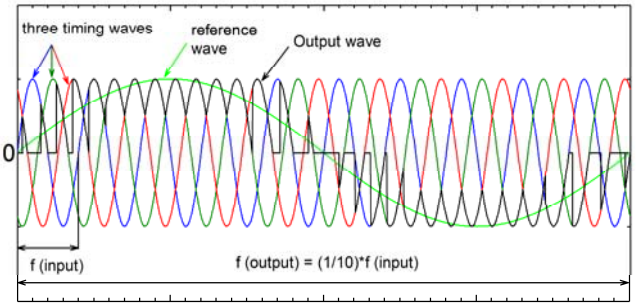

Figure 6. Output waveform of the cycloconverter

VI. Power Control

In order to decouple the active and reactive powers, the stator flux victor will be aligned with d-axis Φ_{sd}, ($\Phi_{sd} = \Phi_s$ and $\Phi_{sq} = 0$). By neglecting resistances of the stator phases the stator voltage will be expressed by [25], [26]:

$$\begin{cases} V_{sd} = 0 \\ V_{sq} = V_s \approx w_s \cdot \phi_s \end{cases} \quad (19)$$

The expressions of the statoric currents are written as:

$$\begin{cases} I_{sd} = \dfrac{\phi_{sd} - M \cdot I_{rd}}{L_s} \\ I_{sq} = -\dfrac{M}{L_s} \cdot I_{rq} \end{cases} \quad (20)$$

By replacing these currents in the rotor fluxes equations, we obtain:

$$\begin{cases} \phi_{rd} = \sigma \cdot L_r \cdot I_{rd} + \dfrac{M}{L_s} \cdot \phi_{sd} \\ \phi_{rq} = \sigma \cdot L_r \cdot I_{rq} \end{cases} \quad (21)$$

With σ is the leakage coefficient, defined by:

$$\sigma = 1 - \frac{M^2}{L_s \cdot L_r} \quad (22)$$

The rotor voltages can be written according to the rotor currents as:

$$\begin{cases} V_{rd} = R_r \cdot I_{rd} + \sigma \cdot L_r \cdot \dfrac{dI_{rd}}{dt} - s \cdot w_s \cdot \sigma \cdot L_r \cdot I_{rq} \\ V_{rq} = R_r \cdot I_{rq} + \sigma \cdot L_r \cdot \dfrac{dI_{rq}}{dt} + s \cdot w_s \cdot \sigma \cdot L_r \cdot I_{rd} + s \cdot \dfrac{M \cdot V_s}{L_s} \end{cases} \quad (23)$$

With s is the slip of the DFIG. And the active and reactive stator powers of the DFIG are expressed by:

$$\begin{cases} P_s = -V_s \cdot \dfrac{M}{L_s} \cdot I_{rq} \\ Q_s = \dfrac{V_s^2}{w_s \cdot L_s} - V_s \cdot \dfrac{M}{L_s} \cdot I_{rd} \end{cases} \quad (24)$$

Then the electromagnetic torque is written as:

$$T_{em} = -p \cdot \frac{M}{L_s} \cdot \phi_{sd} \cdot I_{rq} \quad (25)$$

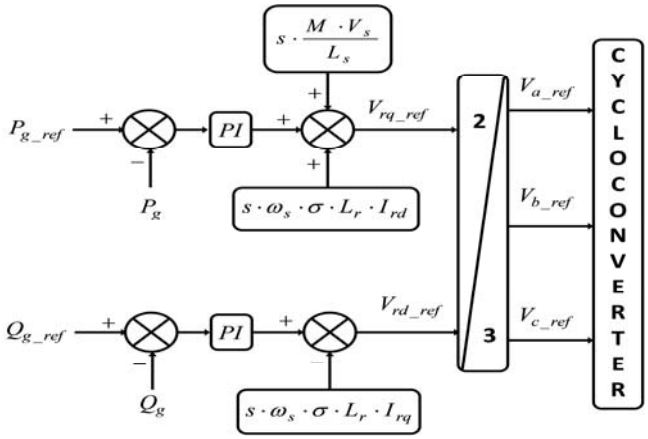

Figure 7. Block diagram of power control

For relatively weak sleep values and by neglecting the voltage drops, the grid active and reactive powers are simplified into [14]:

$$\begin{cases} P_g = (s-1) V_s \cdot \dfrac{M}{L_s} \cdot I_{rq} \\ Q_g = \dfrac{V_s^2}{w_s \cdot L_s} + (s-1) V_s \cdot \dfrac{M}{L_s} \cdot I_{rd} \end{cases} \quad (26)$$

The reference value of the active power exchanged between the wind generator and the grid is generated by MPPT control (Fig. 4), and it's given by:

$$P_{g\_ref} = T_{em\_ref} \cdot \Omega_{mec} \quad (27)$$

The reference grid reactive power, Q_{g_ref} is fixed to zero value to maintain the power factor at unity.

The detailed scheme of the studied system is illustrated in Fig. 8.

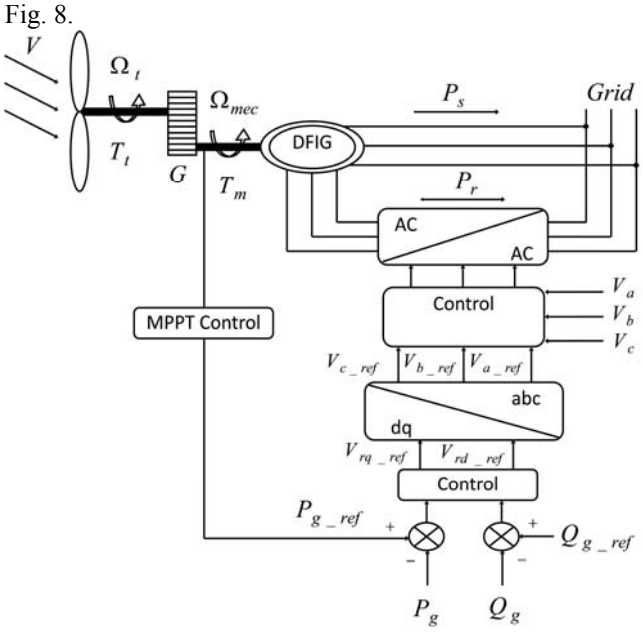

Figure 8. Detailed scheme of the studied device

VII. Results and Discussion

Simulation of the proposed system has been realized using Matlab/Simulink. The parameters of the WECS are given in appendix A [27].

The DFIG is connected directly through its stator and controlled through its rotor by cycloconverter.

To control the power exchanged between the wind generator and the grid, stator flux oriented control technique is applied. The reference value P_{g_ref} of the grid active power is determined by (27), and the reference of the reactive power is maintained zero to guarantee unity power factor.

We have applied to the wind turbine a variable wind speed between 10 and 14.06 m/s, as represented in Fig. 9.

The variation of the mechanical speed of the DFIG is represented in Fig. 10.

Figure 11 shows both the grid active and reactive powers and their references.

The stator and rotor active powers are given in Fig. 12.

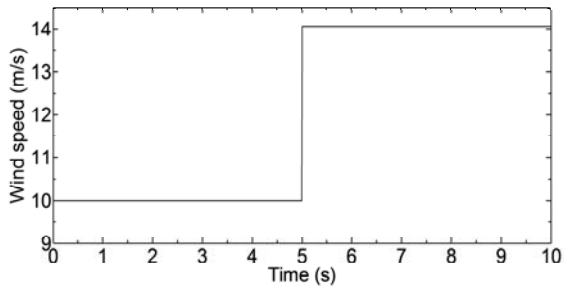

Figure 9. Wind speed

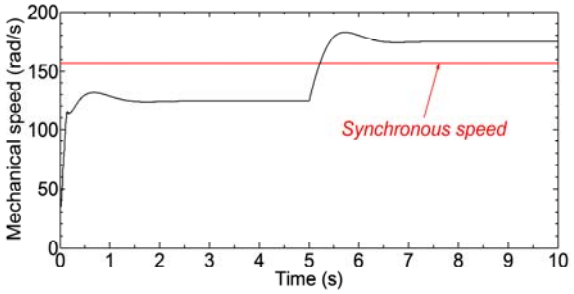

Figure 10. Mechanical speed

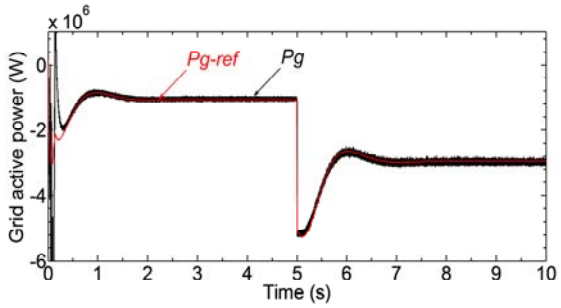

Figure 11a. Grid active power

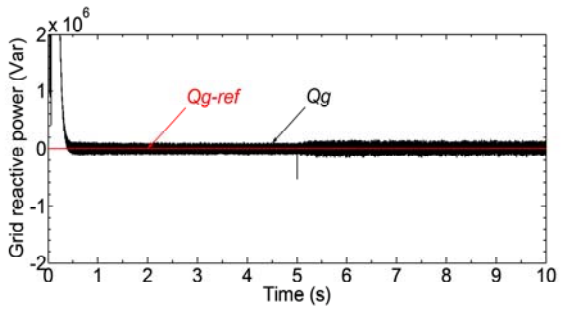

Figure 11b. Grid reactive power

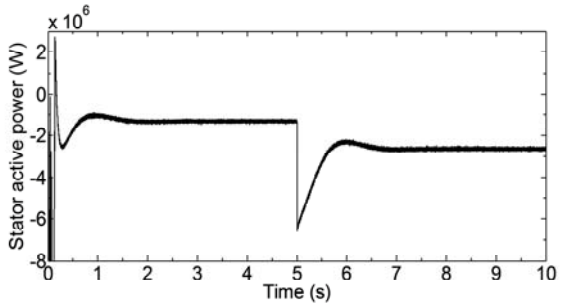

Figure 12a. Stator active power

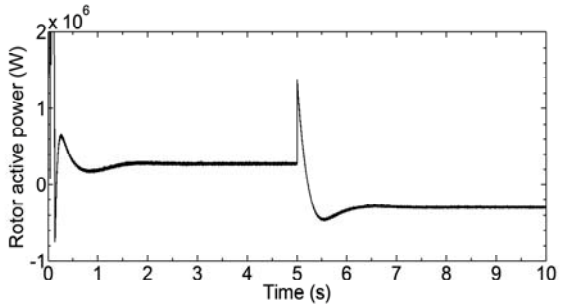

Figure 12b. Rotor active power

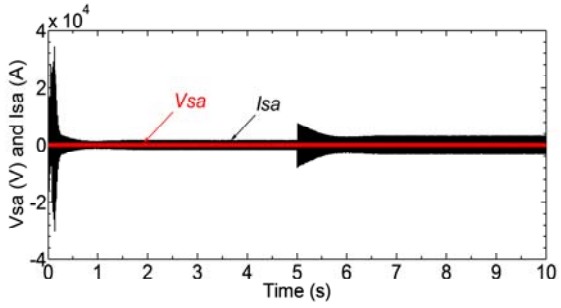

Figure 13a. Stator phase voltage and current

Figure 13 gives the simple waveforms of the stator phase current and voltage, and their zoom. The three phases of the rotor currents waveforms and their zoom are represented in Fig. 14.

Finally, Fig. 15 illustrates the zoom of the rotor phase voltage and current waveforms in the sub and super-synchronous modes.

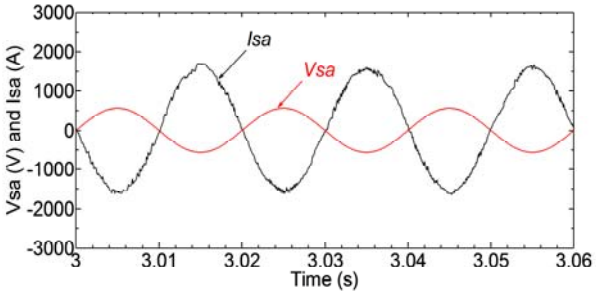

Figure 13b. Zoom of the stator phase voltage and current

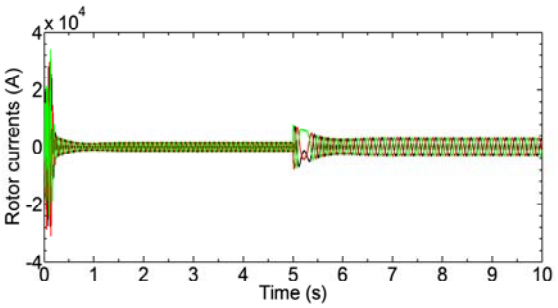

Figure 14a. Rotor currents

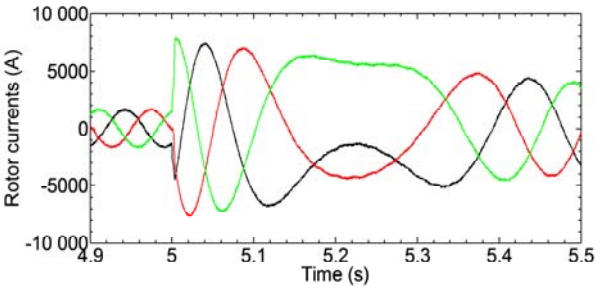

Figure 14b. Transition of the rotor currents from sub-synchronous to super-synchronous mode

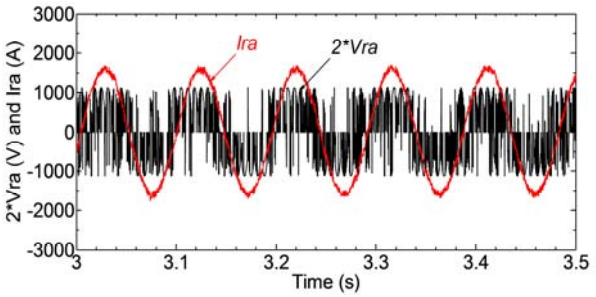

Figure 15a. Zoom of the rotor phase voltage and current in the sub-synchronous mode

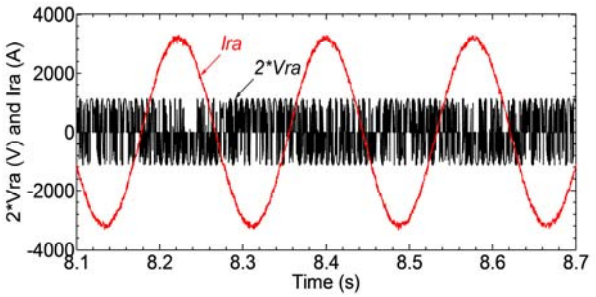

Figure 15b. Zoom of the rotor phase voltage and current in the super-synchronous mode

The mechanical speed in Fig. 10 varies according to the wind speed. In Fig. 11 the grid active and reactive powers follow their references; this figure validates the independent

control of these powers. No reactive power is provided to the grid; this implies that the DFIG supplies the grid only with active power.

The power injected to the grid is the sum of the stator and rotor powers.

The rotor power (P_r) in Fig. 12b operating in two modes. The first one is in sub-synchronous mode ($w < w_s$), P_r is positive because the rotor absorbs power from the grid. The second one is in super-synchronous mode ($w > w_s$), P_r is negative because the rotor provides power to the grid.

In both modes the stator active power is generated from the DFIG and delivered to the grid.

The frequency of the rotor currents in Fig. 14a is low and varies according to the wind speed variations.

Figure 14b shows the transition of the DFIG from sub-synchronous mode to super-synchronous mode.

Figure 15 validates previous results because in Fig.15a the angle between the rotor phase voltage and current is below 90°, which means that the power factor is positive (P_r>0; sub-synchronous mode), and in Fig. 15b the angle between the rotor phase voltage and current is above 90°, which means that the power factor is negative (P_r<0; super-synchronous mode).

VIII. Conclusion

In this work, we have presented a complete WECS made with DFIG and cycloconverter. The stator of the DFIG is connected directly to the grid while the rotor is connected and controlled through three phase cycloconverter. The MPPT performance of the system is tested. The active and reactive powers, exchanged between the wind generator and the grid, are controlled independently through the cycloconverter by using stator-flux oriented control technique and cosine-wave crossing technique. Simulation results are proved the efficiency, demonstrated the ability to operate in two quadrant modes and reduced the cost of the proposed system.

Appendix A

Turbine: $R = 40\ m$, number of blades = 3, $G = 70$

DFIG: $S_n = 3\ MVA$, $U_s = U_r = 690\ V$, $f = 50\ Hz$, $p = 2$ pole pairs, $R_s = 2.97\ m\Omega$, $R_r = 3.82\ m\Omega$, $L_s = 12.241$ mH, $L_r = 12.177\ mH$, $M = 12.12\ mH$, $J = 116\ kg\ m^2$.

References

[1] V. C. Ganti, B. Singh, S. K. Aggarwal, and T. C. Kandpal, ''DFIG-based wind power conversion with grid power leveling for reduced gusts,'' IEEE Trans. On Sustainable energy, vol. 3, no. 1, January 2012.

[2] A. Tapia, G.Tapia, J. X. Ostolaza and J. R. Saenz, "Modeling and control of a wind turbine driven doubly fed induction generator," IEEE Trans. On Energy conversion, vol. 18, no. 2, June 2003.

[3] M. Tazil, V. Kumar, R.C. Bansal, S. Kong, Z.Y. Dong, W. Freitas and H.D. Mathur, "Three-phase doubly fed induction generators: an overview," IET Electric power applications, vol. 4, pp 75-89, 2010.

[4] H. S. Kim and D. D. Chuan Lu, "Review on wind turbine generators and power electronic converters with the grid-connection issues,'' Universities power engineering conference (AUPEC), 20th Australasian, 1-6, 2010.

[5] F. Iov, M. Ciobotaru and F. Blaabjerg, "Power electronics control of wind energy in distributed power systems," Optimization of electrical and electronic equipment, 11th International conference, 2008.

[6] H. Li, Z. Chen and J. K. Pedersen, "Optimal power control strategy of maximizing wind energy tracking and conversion for VSCF doubly fed induction generator system," Power electronics and motion control conference, IPEMC, 2006.

[7] D. Aouzellag, K. Ghedamsi and E.M. Berkouk, "Network power flux control of a wind generator," Renewable energy J 2009, 34:615–622.

[8] K. Ghedamsi and D. Aouzellag, "Improvement of the performances for wind energy conversions systems," Electrical power and energy systems J 2010, 32: 936–945.

[9] A. K. Chattopadhyay, ''Cycloconverters and cycloconverter-fed drives: A review," J. Indian Inst. Sci., vol. 77, pp 397–419, Sep-Oct. 1997.

[10] S. Miyazawa, F. Nakamura and N. Yamada, "Effective approximation suitable for the control algorithm of microprocessor based cycloconverter," IEE Proceedings., vol.135, Pt.B, no. 3, May 1988.

[11] F. Poitiers, T. Bouaouiche and M. Machmoum, "Advanced control of a doubly-fed induction generator for wind energy conversion," Electric power systems research J 2009, 79:1085-1096.

[12] F. Hachicha and L. Krichen, ''Rotor power control in doubly fed induction generator wind turbine under grid faults,'' Energy J 2012, 44: 853–861.

[13] M. V. Kazemi, A. S. Yazdankhah and H. M. Kojabadi, "Direct power control of DFIG based on discrete space vector modulation," Renewable energy J 2010, 35:1033–1042.

[14] N. Taib, B. Metidji and T. Rekioua, "Performance and efficiency control enhancement of wind power generation system based on DFIG using three-level sparse matrix converter," Electrical power and energy systems J 2013, 53: 287–296.

[15] L. Zhang, C. Watthanasarn ''A matrix converter excited doubly-fed induction machine as a wind power generator,'' IET, 7th international Conference on power electronics and variable speed Drives, 532-537, 1998.

[16] H. Altun, S. Sunter, "Modeling, simulation and control of wind turbine driven doubly-fed induction generator with matrix converter on the rotor side," Springer, Electr. Eng., 95:157–170, 2013.

[17] T. Nakano, H. Ohsawa, and K. Endoh, "A high-performance cycloconverter-fed synchronous machine drive system," IEEE Trans. On Industry Applications, vol. IA-20, no. 5, 1984.

[18] Y. Liu, G. T. Heydt and R.F. Chu, "The power quality impact of cycloconverter control strategies," IEEE Trans. On Power delivery, vol. 20, no. 2, April 2005.

[19] M. Boutoubat, L. Mokrani and M. Machmoum, "Control of a wind energy conversion system equipped by a DFIG for active power generation and power quality improvement," Renewable energy J 2013, 50:378–386.

[20] C. Y. Tang, Y. Guo and J. N. Jiang, "Nonlinear dual-mode control of variable-speed wind turbines with doubly fed induction generators," IEEE Trans. On Control Systems Technology, vol. 19, no. 4, July 2011.

[21] A.A. El-Sattar, N.H. Saad and M.Z. Shams El-Dein, "Dynamic response of doubly fed induction generator variable speed wind turbine under fault," Electric power systems research J 2008, 78:1240–1246.

[22] A. Gaillard, ''Système éolien basé sur une MADA: contribution à l'étude de la qualité de l'énergie électrique et de la continuité de service,'' PhD thesis, University of Henri Poincaré, Nancy-I, 30 April 2010.

[23] D. Kairous and R. Wamkeue, "DFIG-based fuzzy sliding-mode control of WECS with a flywheel energy storage," Electric power systems research J 2012, 93:16–23.

[24] A. M. Kassem, K. M. Hasaneen and A. M. Yousef, "Dynamic modeling and robust power control of DFIG driven by wind turbine at infinite grid," Electrical power and energy systems J 2013; 44; 375–382.

[25] Y. Bekakra and D. Ben Attous, ''Sliding mode controls of active and reactive power of a DFIG with MPPT for variable speed wind energy conversion,'' Australian journal of basic and applied sciences, vol. 5, no. 12, pp. 2274-2286, 2011.

[26] L. Jerbi, L. Krichen and A. Ouali, "A fuzzy logic supervisor for active and reactive power control of a variable speed wind energy conversion system associated to a flywheel storage system," Electric power systems research J 2009, 79:919-925.

[27] A. Gaillard, P. Poure, S. Saadate, M. Machmoum, ''Variable speed DFIG wind energy system for power generation and harmonic current mitigation,'' Renew Energy J 2009; 34:1545–1553.